Prepared for submission to JCAP

Cosmic Shear constraints from HSC Year 3 with clustering calibration of the tomographic redshift distributions from DESI

J. Choppin de Janvry [1,2] B. Dai, [3] S. Gontcho A Gontcho, [1,4] U. Seljak, [1,2] T. Zhang [5]

[1] Physics Division, Lawrence Berkeley National Laboratory, Berkeley, CA 94720, USA
[2] Department of Physics, University of California, Berkeley, CA 94720, USA
[3] School of Natural Sciences, Institute for Advanced Study, 1 Einstein Drive, Princeton, New Jersey 08540, USA
[4] Department of Astronomy, University of Virginia, Charlottesville, VA 22904, USA
[5] Department of Physics and Astronomy and PITT PACC, University of Pittsburgh, Pittsburgh, PA 15260, USA

E-mail: jean.choppindejanvrydev@gmail.com, biwei@ias.edu, satya@virginia.edu, useljak@berkeley.edu, tq.zhang@pitt.edu

Abstract. We reanalyze cosmological constraints from Hyper Suprime-Cam (HSC) Y3 shear-shear correlation function using new calibration of the tomographic redshift distribution via the clustering redshifts method with DESI spectroscopy presented in Choppin de Janvry *et al.* (2025a) [1]. We present both importance sampling of the original MCMC chains by HSC, applying the weights of our newly calibrated Δz priors, as well as full MCMC analysis with new photometric redshift distributions, finding consistent results between the two. We obtain the growth of structure parameter $S_8 \equiv \sigma_8\sqrt{\Omega_m/0.3} = 0.805 \pm 0.018$, compared to previous HSC Y3 result of $S_8 = 0.769^{+0.031}_{-0.034}$, which is a 1.8 reduction of error due to the improved clustering redshift calibrations, with the central value shifting considerably higher towards Planck cosmology. With the new photometric redshift calibration, HSC Y3 has comparable constraining power to the recent KIDS Legacy and DES Y3. Combining all three gives $S_8 = 0.813^{+0.009}_{-0.010}$, which can be compared to $S_8 = 0.828 \pm 0.012$ from CMB lensing. Overall there is no evidence for deviation from Planck on S_8 in any of the weak lensing analyses, and combining galaxy lensing with CMB lensing gives a sub-percent constraint $S_8 = 0.818 \pm 0.007$, comparable in both precision and value to the most recent Planck+ACT+DESI constraint $S_8 = 0.812 \pm 0.007$.

Contents

1 Introduction

Weak gravitational lensing (WL) causes subtle distortion of observed galaxy shapes due to the gravitational influence of intervening large-scale structures along the line of sight. By statistically analyzing correlations in these shear distortions across large samples of galaxies, weak lensing surveys provide a powerful probe of the large-scale structure of the universe [2, 3]. These analyses allow us to constrain key cosmological parameters, particularly Ω_m (matter density) and σ_8 (amplitude of matter fluctuations), test the standard ΛCDM model and explore potential deviations from it. WL also causes distortions of cosmic microwave background, with the latest constraints presented in [4]. WL cross-correlation with galaxies can also be combined with galaxy auto-correlation for additional constraints on cosmological parameters. This technique however suffers from potential systematics in the modeling of the cross-correlation coefficient between galaxies and dark matter [5], as well as from observational systematics in the galaxy auto-correlation. In this paper we focus on WL analyses without galaxy clustering.

Several Stage-III weak lensing surveys, including the Hyper Suprime-Cam (HSC; [6]), the Kilo-Degree Survey (KiDS; [7]), and the Dark Energy Survey (DES; [8]), have made significant progress in constraining the cosmological model. However, a persistent feature of these studies has been the so-called S_8 tension: weak lensing surveys have consistently reported values for the lensing amplitude $S_8 \equiv \sigma_8\sqrt{\Omega_m/0.3}$ that are systematically lower than those inferred from cosmic microwave background (CMB) measurements [9] under the ΛCDM framework [10–15]. This discrepancy has led to substantial interest, as it may point to either unknown systematics in the analyses [16, 17] or new physics beyond the standard model [18].

Disentangling these possibilities requires improved control of systematics, particularly in the context of next-generation weak lensing surveys, such as the Rubin Observatory Legacy Survey of Space and Time (LSST) [19], the Nancy Grace Roman Space Telescope [20], and Euclid [21]. These surveys will achieve unprecedented precision, making the mitigation of systematics a crucial priority. Among various systematics, photometric redshift calibration is particularly critical, as errors in redshift distributions propagate directly into biases in the constraints of S_8.

Most recently, the KiDS Legacy survey introduced several enhancements to its analysis, including improved photometric redshift calibration, improved image reduction, and updated intrinsic alignment modeling [22]. Among these, improvements in photometric redshift calibration played a particularly significant role, leading to tighter constraints on cosmological parameters and a notable shift in their S_8 results. The Hyper Suprime-Cam (HSC) Year 3 (Y3) analysis, on the other hand, adopted a wide prior on photometric redshift biases due to limited photo-z calibration in higher redshift bins [12, 13]. This approach allowed HSC to account for uncertainties in the redshift distributions and enabled robust inference, but it also resulted in weaker constraints on S_8. Both KiDS and HSC highlight the critical role of photometric redshift calibration in reducing systematic uncertainties and improving the precision of weak lensing cosmology.

In this work, we reanalyze the HSC Y3 shear-shear correlation function using the updated clustering redshift calibration presented in [1], which leverages spectroscopic data from the Dark Energy Spectroscopic Instrument (DESI, [23, 24]). Our goal is to quantify the impact of this improved redshift calibration on the cosmological constraints derived from HSC Y3 and to explore its implications for the S_8 tension. Our analysis demonstrates that the improved photometric redshift calibration significantly reduces systematic uncertainties, yielding tighter and more robust constraints. Importantly, we find that the updated HSC Y3 results are consistent with Planck CMB measurements, providing a potential resolution to the S_8 tension within the context of HSC. We also compare the updated HSC Y3 constraints with those from KiDS Legacy and DES Y3, examining the consistency among surveys. Additionally, we demonstrate the power of combining galaxy lensing and CMB lensing constraints, achieving sub-percent precision comparable to the Planck × ACT × DESI results.

This paper is organized as follows. In Section 2, we describe the dataset used in this paper, including HSC Y3 shape catalog and the galaxy redshift distribution $n(z)$ calibrated with the DESI data. In Section 3, we present the methodology followed in this analysis to recover cosmological constraints. In Section 4, we present the cosmological constraints and compare to other experiments and surveys. Finally we conclude in Section 5.

2 Datasets

This section describes the datasets and catalogs used in this analysis.

2.1 HSC-SSP PDR3 Shape Catalog

The Hyper Suprime-Cam Subaru Strategic Program (HSC-SSP) is a wide and deep imaging survey conducted by the 8.2-meter Subaru Telescope. The weak lensing shear catalog used in this study is the HSC S19A galaxy shape catalog, i.e., the so-called HSC Year 3 shear catalog[25], an intermediate release between the HSC Public Data Release 2 (PDR2) [26] and HSC Public Data Release 3 (PDR3) [27]. This catalog builds upon $i_{\rm band}$ imaging data obtained from 2014 to 2019 in the Wide fields of the HSC survey, at a mean $i_{\rm band}$ PSF Full-Width of Half-Maximum (FWHM) of $0.59''$ [25]. A conservative $i_{\rm band} < 24.5$ magnitude cut is applied to the dataset. Even with the conservative magnitude cut, the catalog has an effective number density of 19.9 arcmin^{-2}. The geometric footprint of the catalog is split into 6 fields: `HECTOMAP`, `XMM`, `VVDS`, `GAMA09H`, `GAMA15H` and `WIDE12H`.

We adopt consistent tomographic binning to the HSC Y3 cosmic shear [12, 13] and tomographic 2×2pt[28] and 3×2pt analysis[29], which uses $z_{\rm best}$ (defined in [30]) of `DNNz` to assign galaxies into four tomographic bins, using $z = 0.3, 0.6, 0.9, 1.2, 1.5$ as bin edges. In addition, a *quality control cut* is applied to the first and second tomographic bins, which depends on the 95% confidence interval boundaries of the `DNNz` [31] and `Mizuki` [32] photometric redshift algorithms,

$$(z^{\tt DNNz}_{95,\,\rm max} - z^{\tt DNNz}_{95,\,\rm min}) < 2.7 \;\;\&\;\; (z^{\tt Mizuki}_{95,\,\rm max} - z^{\tt Mizuki}_{95,\,\rm min}) < 2.7. \tag{2.1}$$

This selection is performed in order to remove possible double-peak galaxies with photo-z probability density functions reporting multi-modal distributions with a second, smaller peak around $z \sim 3$. The cut removes $\sim 31\%$ of sources in the first bin, and $\sim 8\%$ of sources in the second bin [33].

In the rest of this analysis, when using redshifts outside of the HSC tomographic bins, the quality control cut is applied to all sources with redshifts between $z \sim 0$ and $z \sim 0.3$, which removes about $\sim 16\%$ of the sources within that redshift range. The fiducial redshift value kept to determine if a redshift is included in a bin or not is $z^{\tt DNNz}_{\rm best}$. The $_{\rm best}$ subscript notes the redshift point estimate that minimizes the risk function, $R(z_{\rm p}) = \int P(z) L(\frac{z_{\rm p}-z}{1+z}) {\rm d}z$, based on the individual probability density function $P(z)$ obtained through `DNNz`, and with $L(x)$ a loss function. More details can be found in the following works [30, 31].

2.2 The DESI-Calibrated HSC Y3 $n(z)$

This work presents updated cosmic shear constraints using the calibrated HSC Y3 $n(z)$ distributions obtained in the companion paper [1]. In that work, we use DESI Data Release 1 (DR1) and DR2 to recover the redshift distribution of the four aforementioned tomographic bins by leveraging the spatial clustering of galaxies via the clustering redshifts method. The Dark Energy Spectroscopic Instrument is an eight year multiplexed spectroscopic program started in 2021, conducting a survey of $17,000$ deg^2 of the sky, covering spectroscopic redshift ranges up to $z \sim 4.2$. As such, it provides an unprecedented reference spectroscopic dataset to calibrate photometric redshifts. We measure the angular cross-correlation between the HSC Y3 photometric sample and the DESI spectroscopic reference samples as a function of the spectroscopic redshift. Since galaxies at similar redshifts are physically clustered together, the cross-correlation signal peaks when the photometric and spectroscopic samples overlap in true redshift space, even if the photometric redshift estimates are biased or uncertain.

We analyze how the cross-correlation amplitude varies with spectroscopic redshift, characterize and model systematic biases (including galaxy bias from both the spectroscopic and photometric samples and magnification effects) and finally, we reconstruct a fully DESI-calibrated underlying redshift distribution $n(z)$ of the four tomographic bins of the HSC Y3 photometric sample, displayed in figure 1. In the clustering redshifts analysis, we include two scale cuts used for two-point correlation functions in the $n(z)$ calibration measurement ($0.3 - 3{\rm h}^{-1}$Mpc and $1 - 5{\rm h}^{-1}$Mpc). The smaller scale cut remains the fiducial measurement of this work: however, we make use of both scale cuts for consistency purposes, as presented in section 4. For more details on the methodology followed, we refer the reader to Choppin de Janvry *et al.* (2025a) [1].

3 Method

This section presents the methodology followed in this analysis to recover cosmological constraints. We obtain cosmological constraints in two independent approaches: (a) In Sec-

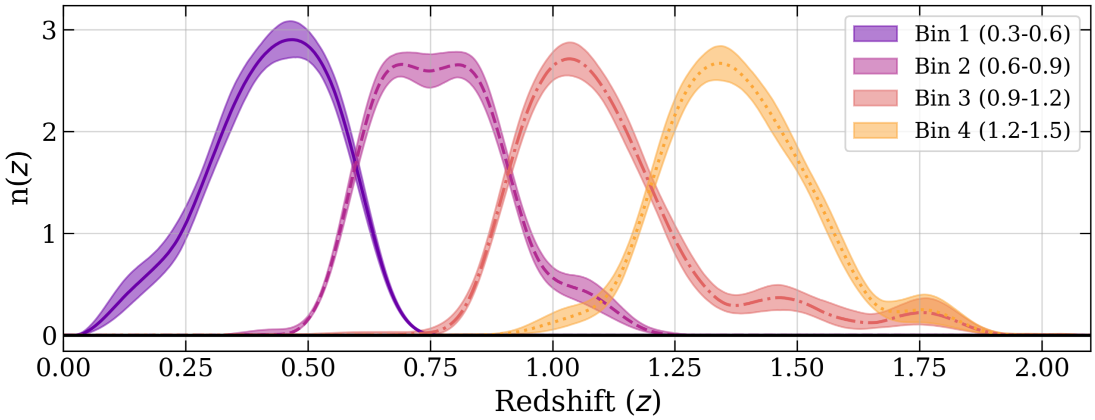

Figure 1: $n(z)$ distributions for each of the 4 tomographic Bins, spanning $z_p \sim 0.3$ to $z_p \sim 1.5$ where z_p is the best estimate of the `DNNz` photo-z algorithm [31] used for tomographic Bin selection, as described in section 2.1. The $n(z)$ for each Bin is displayed with the median posterior sample and the 1σ widths adapted from [1]. Here, the $n(z)$ shown includes all corrections to galaxy bias and magnification effects.

tion 3.1, we apply importance weighting to the redshift distribution parameters of the fiducial HSC Y3 cosmic shear chains [12, 13] based on our new redshift parameter priors; (b) in Section 3.2, we re-run likelihood analysis using the fiducial HSC cosmic shear, with our updated redshift distribution and redshift parameter priors.

3.1 Importance Weighting

Our first approach is to apply importance weights to the photometric redshift shifts Δz on the original chains [13]. The importance weights are only applied to the last two tomographic bins, leveraging the broad uniform ($\mathcal{U}(-1, 1)$) that were applied to the shift parameters in the original analysis. No resampling is applied to the first two bins, because of their narrow gaussian prior already set by original HSC analysis. Bin 1's new calibration presents a slight shift compared to the original $n(z)$ presented in [33], but does not offer significant cosmological information due to being at low redshifts ($0.3 \lesssim z \lesssim 0.6$), so reweighting for bin 1 is neglected. Bin 2's calibration is fully consistent with the calibration presented by Cosmic Shear Ratios [34] and the original calibration [33]. The obtained result is also consistent with the sampling result, as shown in section 4, however, the posterior volume is larger, attributed to larger priors on the first two Bins. The weights $w_i^{(k)}$ derived for Bin $k \in \{3, 4\}$ are:

$$w_i^{(k)} = e^{\left(\frac{\mu_i^{(k)} - \mu^{(k)}}{\sigma^{(k)}}\right)} \tag{3.1}$$

where $\mu_i^{(k)}$ is the mean redshift shift of Bin k of posterior draw i from the original chain, $\mu^{(k)}$, $\sigma^{(k)}$ are respectively the mean and standard deviations of the new prior. Since no weighting is originally applied from the uniform prior, we can multiply the existing weights in MCMC chains with $w_i^{(k)}$.

3.2 Likelihood Analysis

Our second approach towards cosmological parameter inference is to re-run the HSC Y3 fiducial likelihood analysis with our DESI-calibrated redshift distribution $n(z)$ for all four tomographic bins.

The real-space cosmic shear likelihood analysis follows the setup presented in [13] as close as possible, which enables us to highlight the effects caused solely by the photometric redshift calibration. Our analysis setup follows the modeling choices in [13] in terms of the calculation of the Baryonic physics, galaxy intrinsic alignment, shear multiplicative bias, and PSF additive bias. For all parameters besides the photo-z parameters, we follow the choices performed in [12, 13] and implement a total of 23 free parameters. The cosmological inference is implemented in the public software `CosmoSIS`[1] and the configuration files used in this analysis are made available through the common repository for this work and the companion $n(z)$ calibration analysis [1]: github.com/jeanchdjdev/desi-y3-hsc. The priors for all of the 23 parameters are described in table 1. The fixed parameters are given in table 2 in appendix A. For the matter power spectrum, we use the CAMB[2] [35] linear power spectrum emulator, in a divergent approach from using the BACCO suite of emulators [36] [3] used in [13]. It is shown that there is no significant different in cosmology results between CAMB and BACCO emulator for HSC Y3 [13].

The two-point correlation functions (TPCF) of galaxy shear are denoted $\xi_\pm$ [13] and are measured on the shear catalog introduced in section 2.1. We also follow the same formalism when it comes to likelihood calculation, compared to [13]. The scale cut applied in this analysis is the same as [13]: $7.1 < \theta < 56.6$ [arcmin] for $\xi_+(\theta)$, and $31.2 < \theta < 248$ [arcmin] for $\xi_+(\theta)$. We adopted the same covariance matrix calculated by 1404 mock HSC Y3 catalogs. We also apply the same Hartlap factor [37] to the likelihood calculation to account for covariance matrix underestimation due to limited mock catalogs. In the HSC Y3 fiducial pipeline, the S_8 parameter is not sampled and is instead a computed property from the other sampled parameters.

The sampler we used for the likelihood analysis is `pocoMC`[4] [38, 39]. `pocoMC` utilizes the Preconditioned Monte Carlo (PMC) algorithm which offers significant speed-ups over more traditional approaches such as Markov Chain Monte Carlo (MCMC). We verify `pocoMC` accurately recovers the fiducial HSC chains in `CosmoSIS`. 2D posteriors for parameters are obtained with the `getDist`[5] [40] package. Comparatively to [13], this work does not use the `ChainConsumer`[6] [41] package to treat the chains, due to potential biases incorporated by the boundary effects and smoothing of MC samples at the border with Kernel Density Estimation (KDE) mentioned in Appendix A of [13]. However, constraints are also computed with `ChainConsumer` and consistency with `getDist` is confirmed for parameters S_8 and Ω_m.

In this work, the posterior of cosmological parameter constraints is presented in the form of:

$$\text{1D mode}^{+34\%}_{-34\%}\ \text{(MAP)} \tag{3.2}$$

where the 1D mode is the is 1D mode of the marginalized 1D posterior distribution, the MAP is the Maximum A Posteriori point of the chain (i.e. the best fit model, including the

[1] github.com/cosmosis-developers/cosmosis-standard-library
[2] camb.info
[3] baccoemu.readthedocs.io
[4] pocomc.readthedocs.io
[5] getdist.readthedocs.io
[6] samreay.github.io/ChainConsumer/

priors), and the error interval is the asymmetric 34% confidence interval around the mode of the distribution, computed with the cumulative density function. A large deviation between the 1D mode and the MAP is often an indication of prior volume projection effects caused by fitting too many parameters that are not directly observable. The values themselves are presented as obtained by `getDist` using `MCSamples.get1DDensity` and the weights are obtained through the sampling from `pocoMC` or included in the fiducial HSC Y3 chains.

4 Results

In this section, we present the fiducial constraints we obtain from the weak lensing cosmological inference in real space and compare them to other experiments and surveys. Measurements from this analysis are compared to other, comparable measurements in order to obtain precise joint constraints of the growth of structure.

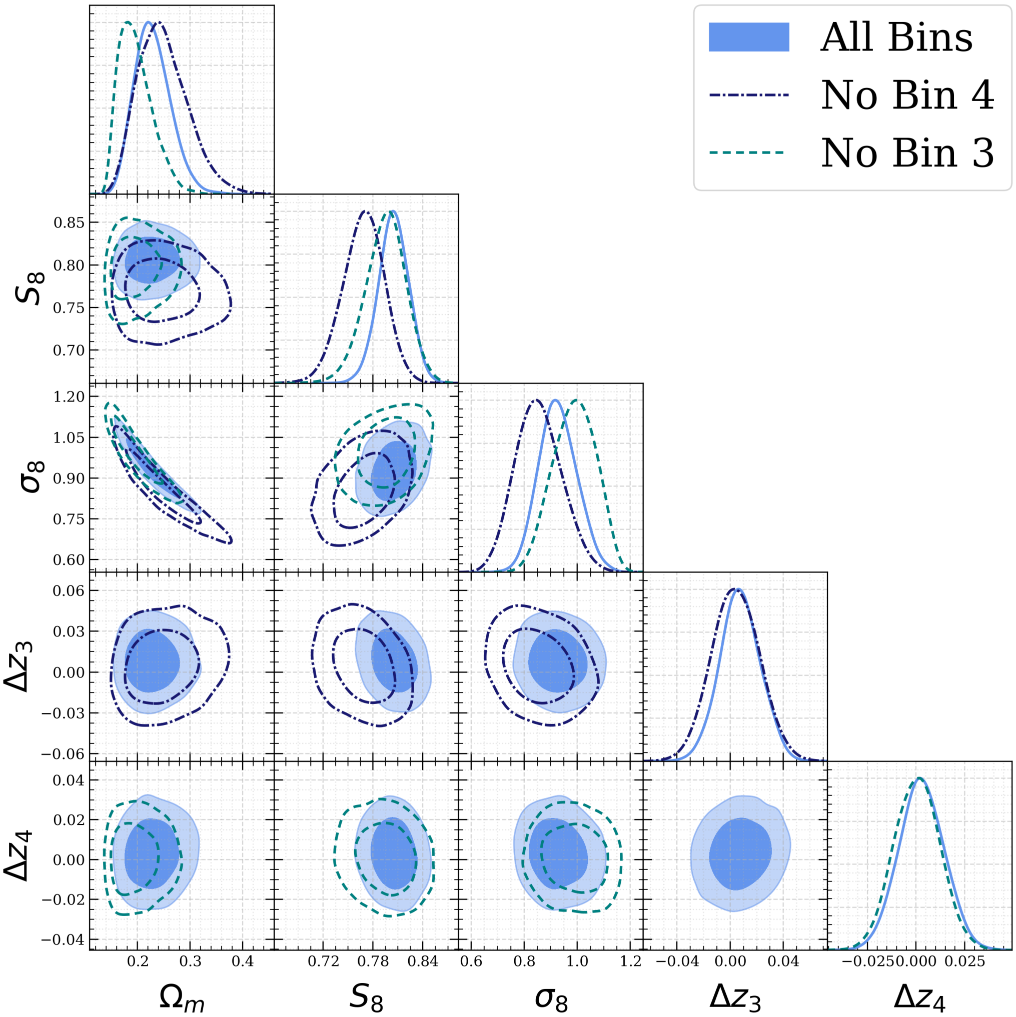

Figure 2: To assess the robustness of the measurement, we exclude Bin 3 and Bin 4 respectively from the chain inference. The measurements are shown to be consistent between the two and consistent with the "All Bins" measurement.

Furthermore, we investigate the robustness of this analysis by comparing the results to importance sampling of the fiducial chains, as well as using different configuration for the tomographic $n(z)$ distributions. We note that following the setup proposed in `CosmoSIS`, the convention used for Δz parameter shifts is opposed to the one presented in the clustering redshift analyses [1, 33] and in the cosmological inference works such as [12, 13, 28, 29]. Here, a positive shift implies that the real $n(z)$ distribution is at higher redshifts than the original, calibrated one proposed in the redshift calibration analyses: the original convention implied the same for negative shifts.

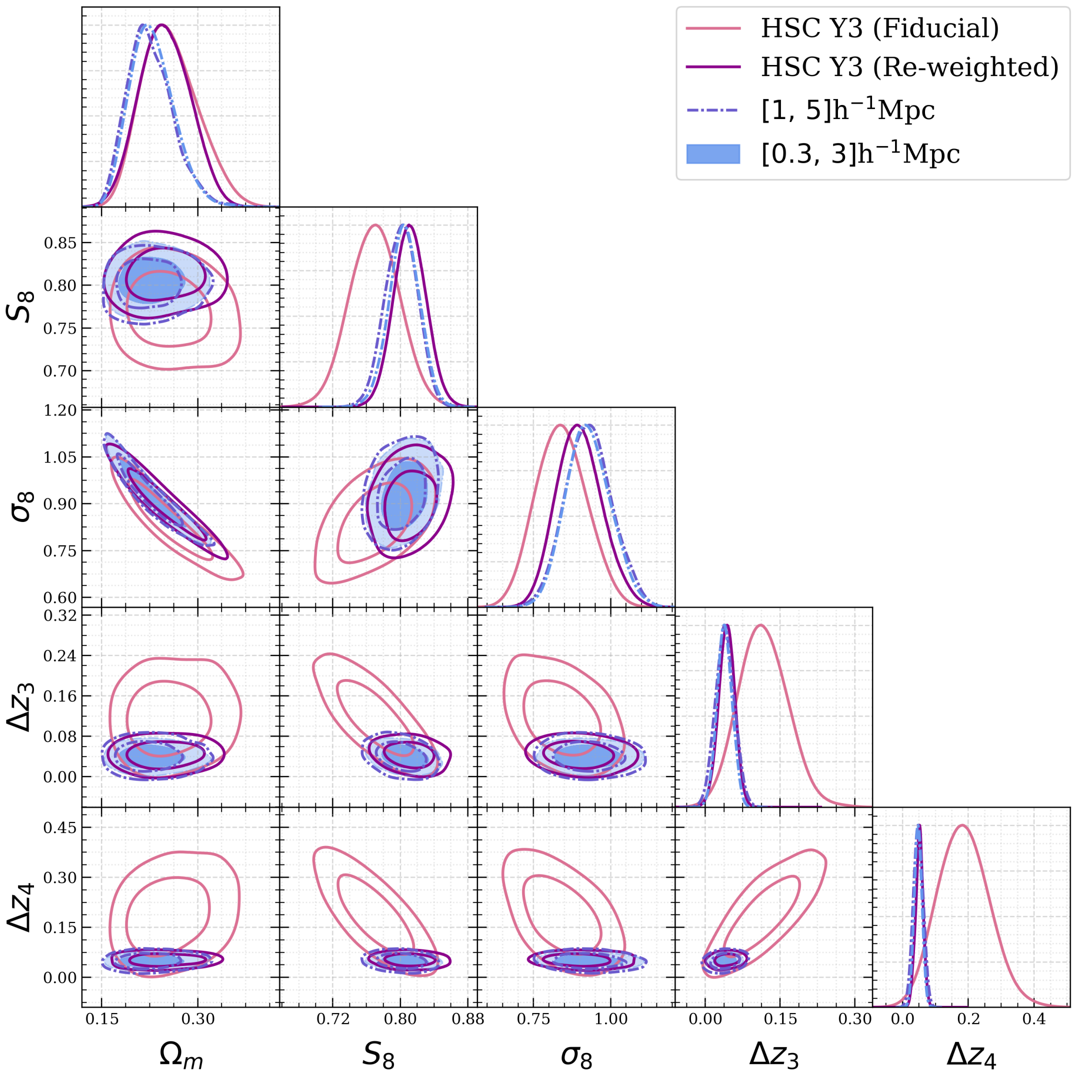

Figure 3: Comparing the sampled results (section 3.2) from the two $n(z)$ set of distributions at different scale cuts with the importance re-weighting (section 3.1) approach in real space and to the HSC Y3 fiducial result. The shift posteriors are artificially shifted by the expectation of the inferred shift in [1], as they are by default centered around 0 for the sampling approach, since new $n(z)$ distributions are used.

Figure 3 compares the joint 2D posteriors for the fiducial result, the $1-5\mathrm{h}^{-1}$Mpc scale cut $n(z)$ result to the importance sampling in real space and the fiducial HSC Y3 result. The underlying $\Delta z_{\{3,4\}}$ shifts lie at 1-2 sigma away from the reported posterior from the HSC Y3. While the shifts are significant in value, they are not statistically inconsistent with the self-calibration method deployed in HSC Y3.

In Figure 2, consistency tests are performed by running cosmological inference while removing information provided by either Bin 3 or Bin 4, and compare to the full run. The resulting corner plot displays consistent measurements between all bins. A preference towards lower Ω_m and higher σ_8 values is noticed when excluding Bin 3, akin to behavior presented in Figure 17 of the two-point correlation analysis [13], but the σ-shifts presented in Figure 4 alleviate concerns of inconsistencies. The lower error bound of the "No Bin 3" chain is underestimated due to the MCMC chain piling up near the boundaries of the prior ($\pi(\Omega_m) \sim \mathcal{U}(0.1, 0.7)$). Furthermore, the obtained value when excluding Bin 3 presents a fairly low value of Ω_m, showing the same trend as what was obtained in the same scenario in the real space analysis [13]. In this work, akin to [12, 13], the constraint on the S_8 parameter is emphasized, due to the strong degeneracies between parameters Ω_m and σ_8.

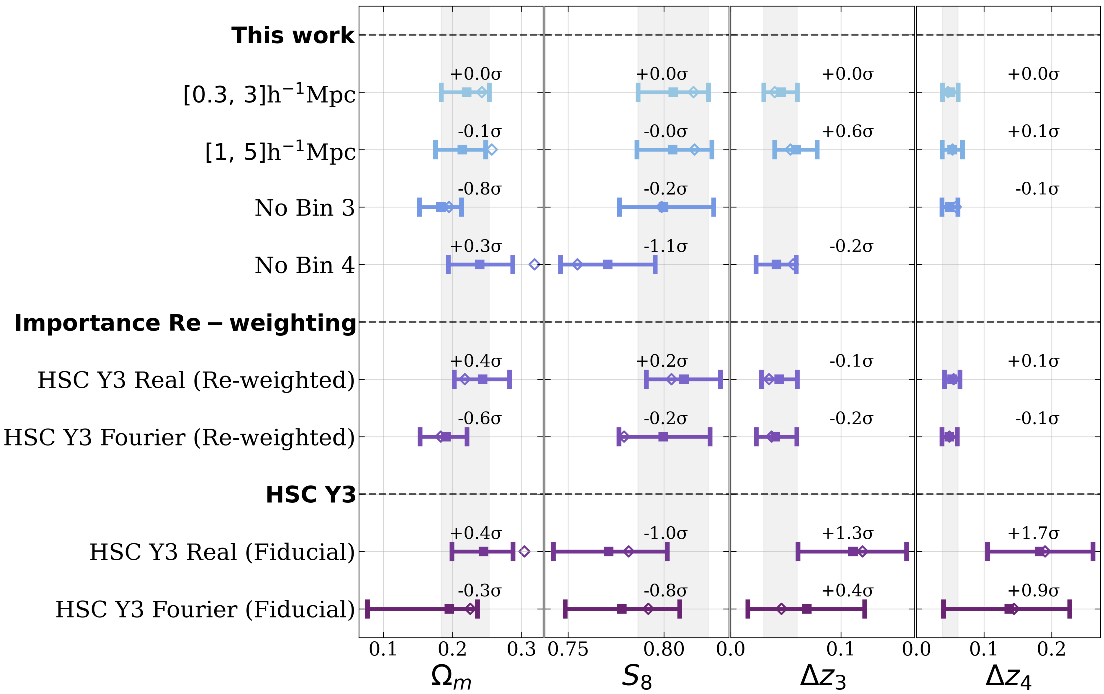

Figure 4: Ω_m, S_8, Δz_3, Δz_4 parameters compared under different measurements. This includes the sampling approach, where the $n(z)$ distributions at two different scale cuts are included, as well as the measurements obtained when excluding either Bin 3 or Bin 4. These are then compared to the importance re-weighting and fiducial results of the Real and Fourier HSC Y3 analyses [12, 13]. The square marker displays the 1D posterior mode obtained with `getDist`. The diamond marker is the Maximum A Posteriori (MAP) value. The background gray area represents the projected fiducial measurement obtained with the $0.3 - 3\mathrm{h}^{-1}\mathrm{Mpc}$ scale cut for the $n(z)$. The $n(z)$ distributions are not the same for HSC Y3 samples (derived from [33]) and this work (from [1]) : the posteriors of this work have been artificially shifted to match the mean of the shifts found in [1].

Table 1: Fiducial parameters and priors for this cosmological analysis. $\mathcal{U}(a, b)$ represents a flat (uniform) prior over bounds $[a, b]$, while $\mathcal{N}(\mu, \sigma)$ represents a Gaussian prior of mean μ and standard deviation σ. S_8 and σ_8 are computed quantities. The values are presented according to equation 3.2. The redshift shifts are relative to our derived distributions, and are centered around zero. Note that baryonic feedback posterior distribution is very non-Gaussian and posterior density has non zero support at zero feedback value of $A_b = 3.13$.

Parameter	Prior	$[\mathbf{0.3},\, \mathbf{3}]\mathrm{h}^{-1}\mathbf{Mpc}$	$[\mathbf{1},\, \mathbf{5}]\mathrm{h}^{-1}\mathbf{Mpc}$
Cosmological Parameters			
$A_s\,(\times 10^9)$	$\mathcal{U}(0.5, 10)$	$3.721^{+1.284}_{-1.820}(2.765)$	$3.730^{+1.371}_{-2.092}(2.922)$
Ω_m	$\mathcal{U}(0.1, 0.7)$	$0.221^{+0.033}_{-0.037}(0.243)$	$0.214^{+0.034}_{-0.039}(0.257)$
σ_8	–	$0.922^{+0.073}_{-0.071}(0.907)$	$0.936^{+0.083}_{-0.071}(0.882)$
S_8	–	$0.805^{+0.018}_{-0.018}(0.815)$	$0.804^{+0.020}_{-0.019}(0.816)$
n_s	$\mathcal{U}(0.87, 1.07)$	$0.900^{+0.053}_{-0.041}(0.885)$	$0.881^{+0.049}_{-0.023}(0.898)$
h_0	$\mathcal{U}(0.62, 0.80)$	$0.662^{+0.052}_{-0.056}(0.746)$	$0.701^{+0.059}_{-0.052}(0.724)$
$\omega_b \equiv \Omega_b h^2$	$\mathcal{U}(0.02, 0.025)$	$0.024^{+0.003}_{-0.002}(0.020)$	$0.020^{+0.002}_{-0.000}(0.024)$
Baryonic Feedback			
A_b	$\mathcal{U}(2, 3.13)$	$2.075^{+0.243}_{-0.128}(2.083)$	$2.041^{+0.226}_{-0.089}(2.137)$
Intrinsic Alignment			
A_1	$\mathcal{U}(-6, 6)$	$0.441^{+0.356}_{-0.334}(0.648)$	$0.432^{+0.369}_{-0.373}(0.503)$
η_1	$\mathcal{U}(-6, 6)$	$-2.478^{+2.884}_{-2.553}(-3.549)$	$-1.943^{+2.853}_{-2.717}(-4.323)$
A_2	$\mathcal{U}(-6, 6)$	$-0.058^{+0.748}_{-0.840}(-0.603)$	$-0.057^{+0.778}_{-0.841}(-0.469)$
η_2	$\mathcal{U}(-6, 6)$	$-1.524^{+3.143}_{-3.149}(-3.915)$	$-1.552^{+3.048}_{-3.511}(-4.782)$
b_TA	$\mathcal{U}(0, 2)$	$0.062^{+0.421}_{-0.135}(0.061)$	$0.067^{+0.441}_{-0.159}(0.163)$
Redshift shifts			
Δz_1	$\mathcal{N}(0, 0.008)$	$-0.002^{+0.008}_{-0.008}(-0.002)$	$-0.003^{+0.013}_{-0.013}(-0.004)$
Δz_1	$\mathcal{N}(0, 0.009)$	$-0.002^{+0.009}_{-0.008}(-0.009)$	$-0.010^{+0.012}_{-0.011}(-0.027)$
Δz_3	$\mathcal{N}(0, 0.020)$	$0.007^{+0.015}_{-0.016}(0.001)$	$0.020^{+0.019}_{-0.019}(0.015)$
Δz_4	$\mathcal{N}(0, 0.012)$	$0.002^{+0.011}_{-0.012}(-0.001)$	$0.005^{+0.015}_{-0.015}(0.005)$
Shear calibration			
Δm_1	$\mathcal{N}(0, 0.01)$	$0.000^{+0.011}_{-0.010}(-0.009)$	$0.001^{+0.011}_{-0.010}(-0.003)$
Δm_2	$\mathcal{N}(0, 0.01)$	$-0.003^{+0.010}_{-0.009}(0.001)$	$-0.005^{+0.010}_{-0.010}(-0.003)$
Δm_3	$\mathcal{N}(0, 0.01)$	$0.000^{+0.009}_{-0.009}(0.001)$	$0.001^{+0.009}_{-0.010}(-0.001)$
Δm_4	$\mathcal{N}(0, 0.01)$	$0.005^{+0.009}_{-0.010}(0.010)$	$0.007^{+0.011}_{-0.009}(0.005)$
PSF systematics			
$\tilde{\alpha}_2$	$\mathcal{N}(0, 1)$	$0.075^{+0.997}_{-0.937}(0.159)$	$-0.094^{+0.922}_{-1.093}(-0.109)$
$\tilde{\beta}_2$	$\mathcal{N}(0, 1)$	$0.033^{+0.939}_{-0.965}(0.160)$	$0.102^{+0.979}_{-0.951}(-0.120)$
$\tilde{\alpha}_4$	$\mathcal{N}(0, 1)$	$-0.347^{+0.910}_{-0.938}(-1.281)$	$-0.271^{+0.913}_{-0.942}(-0.461)$
$\tilde{\beta}_4$	$\mathcal{N}(0, 1)$	$-0.005^{+1.027}_{-0.961}(0.271)$	$-0.091^{+0.983}_{-1.026}(-0.014)$

Figure 4 compares the relative shifts to the fiducial measurement of this work under different scenarios. We perform consistency tests with Bin 3 or Bin 4 excluded and using the distributions inferred with the larger scale cut ($1-5\text{h}^1\text{Mpc}$) obtained in [1]. The importance re-weighting results obtained with the method described in section 3.1 are shown next. The measured shift in the Δz bins in the context of the importance re-weighting, the $1-5\text{h}^1\text{Mpc}$ distributions or in the context of the HSC Y3 fiducial $n(z)$ derived in [33] cannot be strictly compared to the $n(z)$ shifts found in this work, since the $n(z)$ distributions themselves differ. Lastly, the importance re-weighting of the HSC Y3 chains means constraining the originally broad uniform $\mathcal{U}(-1,1)$ prior over Δz_3, Δz_4 to a stricter gaussian prior. We note that reweighting leads to a fairly low number of effective sample size with respect to the original chain, leading to noisy 2D posteriors.

The priors for all sampled parameters in the case of the fiducial $n(z)$ is reported in table 1, alongside the posterior sampled values obtained for the other scale cuts. We note that the redshift Δz_i priors depend on the chosen scale cut, as mentioned in appendix A. Figure 5 compares other recent S_8 constraints with respect to the constraints obtained in this work. The most recent non-lensing CMB result is Planck × ACT × DESI DR2 constraints obtained from the power spectra measurements of ACT DR6 presented in [42]. The most recent CMB lensing result is Planck × ACT × SPT (CMBL): the CMB lensing constraints obtained from combining Planck, ACT and SPT maps in work [4]. We also show measurements obtained with weak lensing from KiDS-Legacy [22], DES [43, 44], HSC Y3 (in both real [13] and Fourier [12] space), and the combined measurement of KiDS-Legacy and DES presented in [22]. Results from this paper derived from the $n(z)$ re-calibration performed in [1] are presented next. The two scale cuts with all bins are measured with `pocoMC` sampling, as discussed in Section 3.2. We also show results from importance re-weighting of the files. Finally, we combine KIDS and DES with the fiducial measurement of this work ($S_8 = 0.805 \pm +0.018$ (0.815)) to KiDS and DES, obtaining $S_8 = 0.813^{+0.009}_{-0.010}$ under the assumption that the surveys are independent. HSC Y3 has about 60% area overlap with DES and KIDS, with effective density for HSC of 16 galaxies/arcmin^2, versus about 6 galaxies/arcmin^2 for DES and KIDS [45]. This suggests that about 20% of HSC galaxies are already included in KIDS+DES. However, because these are brighter they are more likely to be in the first HSC tomographic redshift bin (which has 5 galaxies/arcmin^2). This tomographic bin has very little constraining power for HSC due to its low shear signal. Most of cosmological constraining power is coming from bins 2-4, which are effectively independent of DES+KIDS. Nevertheless, our analysis should be considered preliminary. Finally, we further combine into the joint WL constraint with CMB Lensing information, obtaining $S_8 = 0.818 \pm 0.007$, a sub-percent constraint on S_8. This result can be compared to the most recent Planck × ACT × DESI DR2 ($S_8 = 0.812 \pm 0.007$), finding a similar value in both the mean and variance: we find no significant discrepancy between the two in the mean, and the combined constraining power of WL surveys is now comparable to that of the CMB.

5 Conclusion

In this work, we provide cosmological constraints from cosmic shear with DESI-calibrated HSC Year 3 $n(z)$ tomographic bin distributions. We find $S_8 = 0.805 \pm 0.018$ when using information from clustering redshifts in the re-calibration analysis. Leveraging clustering information from quasars and emission line galaxies (above $z \gtrsim 0.8$), the calibrated priors of Bins 3 and Bin 4 are shown to be significantly less biased compared to the self-calibration

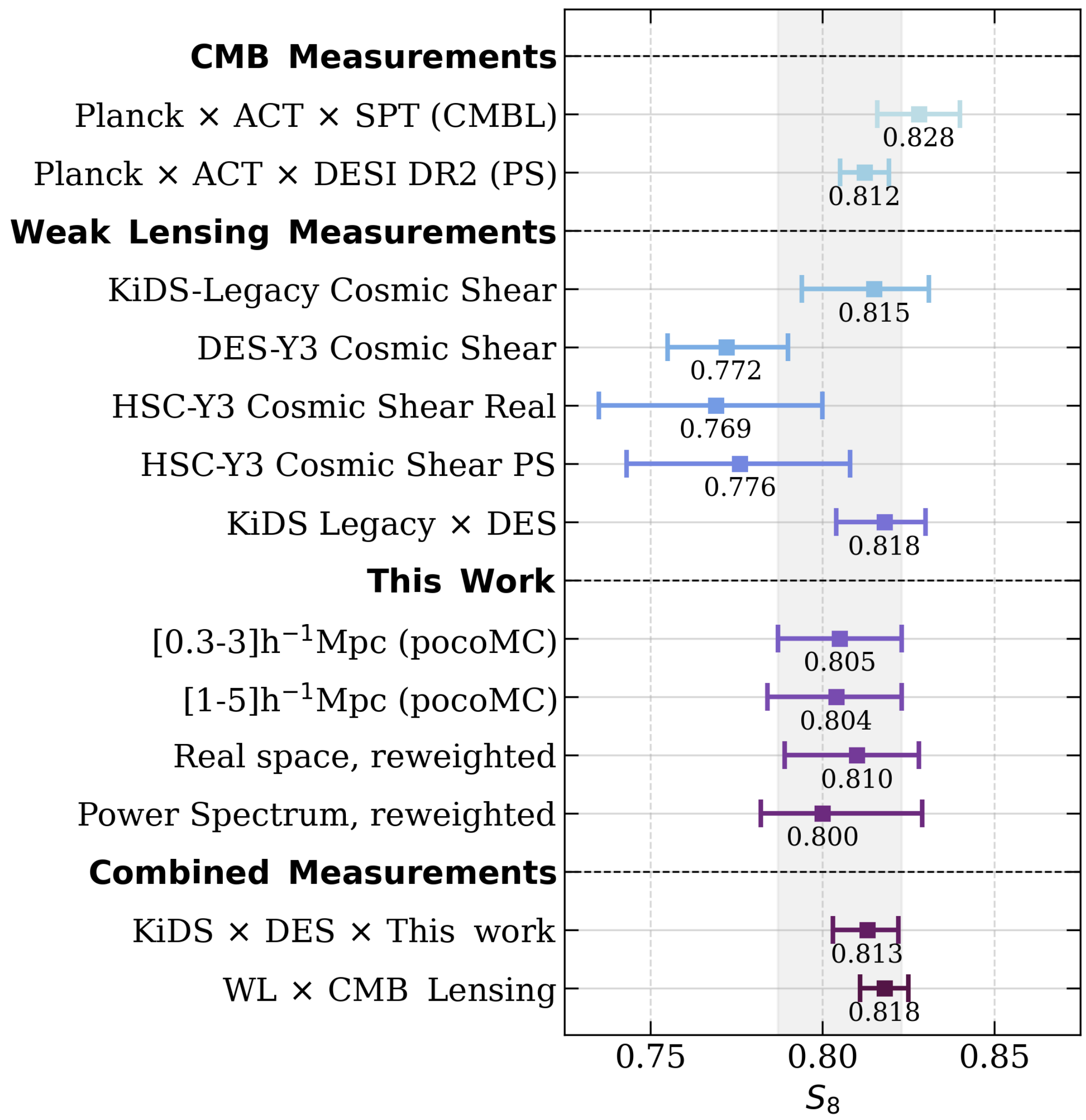

Figure 5: Measurements from different surveys measuring the growth of structure, from *CMB Measurements* and *Weak Lensing Measurements*. The results are further compared to the results obtained in this work, as well as combined with the S_8 constraints obtained. The source of every cited measurement is discussed in text.

shift posteriors, as displayed in Figure 3 and Figure 4. While our derived photometric bias is not zero, our results show that the original photometric calibrations of HSC are not very biased.

Our result can be compared to previous HSC Y3 result of $S_8 = 0.769^{+0.031}_{-0.034}$. Our result gives a 1.8 reduction of error due to the improved clustering redshift calibrations, with the central value shifting considerably higher towards Planck cosmology. Our reanalysis makes HSC competitive with other Stage 3 lensing surveys such as DES [43, 44] and KiDS [22]. Combination with DES and KiDS leads to the combined result $S_8 = 0.813^{+0.009}_{-0.010}$, competitive with the CMB lensing measurements. Further combining galaxy lensing with CMB lensing leads to the sub-percent $S_8 = 0.818 \pm 0.007$ constraint. In contrast to the $S_8 \sim 2\sigma$ tension with CMB results originally found for HSC Y3 in [12, 13], the findings of this work show no evidence of significant deviations from Planck S_8 measurements for HSC and for HSC combined with DES and KIDS Legacy. The compatibility with Planck results from the measurements of this analysis as well as the joint constraints from the Stage III weak lensing surveys suggest that the suspected "S_8 tension" [46] was primarily systematics driven and has now been largely eliminated from all of the WL analyses. We emphasize that we focus on WL only analyses here: the analyses combining WL with galaxy clustering have additional potential systematics that may complicate their interpretation, and are not included here.

Our results suggest that clustering calibration of WL photometric redshifts plays a crucial role in achieving the goals of WL surveys. We expect the same to apply to the upcoming weak lensing releases of Stage III surveys such as the Dark Energy Survey Year 6 and HSC Public Data Release 4, as well as the upcoming releases of Stage IV weak lensing surveys such as Euclid [47] and the Vera C. Rubin Legacy Survey of Space and Time [19]. Assuming photometric redshifts can be reliably calibrated with the spectroscopic surveys such as DESI, these will provide new percent-level constraints on the growth of structure of the universe, further validating the standard cosmological model.

The code used for this work, the chains, and all the data to replicate the figures of this paper is made publicly available at github.com/jeanchdjdev/desi-y3-hsc. For the specific cosmic shear analysis, this work is compiled under the `cosmic_shear` directory of the repository.

Acknowledgments

JCdJ acknowledges support from Fondation CentraleSupélec and Fondation Ailes de France. BD acknowledges support from the Ambrose Monell Foundation, the Corning Glass Works Foundation Fellowship Fund, and the Institute for Advanced Study. SGG acknowledges that this work was performed in part at the Aspen Center for Physics, which is supported by National Science Foundation grant PHY-2210452 and a grant from the Alfred P Sloan Foundation (G-2024-22395). US is supported by NSF CDSE grant number AST-2408026 and NASA TCAN grant number 80NSSC24K0101. TZ is supported by Schmidt Sciences.

The Hyper Suprime-Cam (HSC) collaboration includes the astronomical communities of Japan and Taiwan, and Princeton University. The HSC instrumentation and software were developed by the National Astronomical Observatory of Japan (NAOJ), the Kavli Institute for the Physics and Mathematics of the Universe (Kavli IPMU), the University of Tokyo, the High Energy Accelerator Research Organization (KEK), the Academia Sinica Institute for Astronomy and Astrophysics in Taiwan (ASIAA), and Princeton University. Funding was contributed by the FIRST program from the Japanese Cabinet Office, the Ministry of Education, Culture, Sports, Science and Technology (MEXT), the Japan Society for the Promotion of Science (JSPS), Japan Science and Technology Agency (JST), the Toray Science Foundation, NAOJ, Kavli IPMU, KEK, ASIAA, and Princeton University. This paper makes use of software developed for Vera C. Rubin Observatory. We thank the Rubin Observatory for making their code available as free software at `http://pipelines.lsst.io/`. This paper is based on data collected at the Subaru Telescope and retrieved from the HSC data archive system, which is operated by the Subaru Telescope and Astronomy Data Center (ADC) at NAOJ. Data analysis was in part carried out with the cooperation of Center for Computational Astrophysics (CfCA), NAOJ. We are honored and grateful for the opportunity of observing the Universe from Maunakea, which has the cultural, historical and natural significance in Hawaii.

This analysis made use of the following software packages: `CosmoSIS` (`https://cosmosis.readthedocs.io/en/latest/`) [48], `pocoMC` (`https://pocomc.readthedocs.io/en/latest/`) [38, 39], `getDist`(`https://getdist.readthedocs.io/en/latest/`)[40], `ChainConsumer` (`https://github.com/Samreay/ChainConsumer`) [41], `matplotlib` [49], `numpy` [50].

A Appendix

In this appendix, we append additional details to the parameters sampled during the cosmological inference runs. The priors are the same as [13], besides for the Δz shift parameters, where we adopt Gaussian priors derived from the companion calibration work led in [1]. The fixed parameters in the cosmology are also conserved and are displayed in table 2. The rest of the 23 free cosmological parameters priors can be found in Table 1.

In table 1, we report the priors used for the fiducial scale cut ($0.3 - 3\text{h}^{-1}$Mpc). The priors used for the lager, $1 - 5\text{h}^{-1}$Mpc scale cut are in order :

- $\Delta z_1 \sim \mathcal{N}(0, 0.013)$
- $\Delta z_2 \sim \mathcal{N}(0, 0.014)$
- $\Delta z_3 \sim \mathcal{N}(0, 0.028)$
- $\Delta z_4 \sim \mathcal{N}(0, 0.016)$

Table 2: Fixed cosmological parameters for inference

Fixed parameters	–
$\sum m_\nu$ (eV)	0.06
w	-1
w_a	0
Ω_k	0
τ	0.0851

References

[1] J. Choppin De Janvry, S. Gontcho A Gontcho, U. Seljak et al., "Full calibration of the tomographic redshift distribution from the HSC PDR3 Shape Catalog with DESI.".

[2] M. Bartelmann and P. Schneider, *Weak gravitational lensing*, *Physics Reports* **340** (2001) 291.

[3] M. Kilbinger, *Cosmology with cosmic shear observations: a review*, *Reports on Progress in Physics* **78** (2015) 086901.

[4] F.J. Qu, F. Ge, W.L.K. Wu, I. Abril-Cabezas, M.S. Madhavacheril, M. Millea et al., *Unified and consistent structure growth measurements from joint act, spt and Planck cmb lensing*, 2504.20038.

[5] J. Guzik and U. Seljak, *Galaxy-dark matter correlations applied to galaxy-galaxy lensing: predictions from the semi-analytic galaxy formation models*, MNRAS **321** (2001) 439 [astro-ph/0007067].

[6] H. Aihara, N. Arimoto, R. Armstrong, S. Arnouts, N.A. Bahcall, S. Bickerton et al., *The hyper suprime-cam ssp survey: overview and survey design*, *Publications of the Astronomical Society of Japan* **70** (2018) S4.

[7] K. Kuijken, C. Heymans, H. Hildebrandt, R. Nakajima, T. Erben, J.T.A. de Jong et al., *Gravitational lensing analysis of the Kilo-Degree Survey*, MNRAS **454** (2015) 3500 [1507.00738].

[8] Dark Energy Survey Collaboration, T. Abbott, F.B. Abdalla, J. Aleksić, S. Allam, A. Amara et al., *The Dark Energy Survey: more than dark energy - an overview*, MNRAS **460** (2016) 1270 [1601.00329].

[9] Planck Collaboration, N. Aghanim, Y. Akrami, M. Ashdown, J. Aumont, C. Baccigalupi et al., *Planck 2018 results. VI. Cosmological parameters*, A&A **641** (2020) A6 [1807.06209].

[10] A. Amon, D. Gruen, M.A. Troxel, N. MacCrann, S. Dodelson, A. Choi et al., *Dark Energy Survey Year 3 results: Cosmology from cosmic shear and robustness to data calibration*, Phys. Rev. D **105** (2022) 023514 [2105.13543].

[11] L.F. Secco, S. Samuroff, E. Krause, B. Jain, J. Blazek, M. Raveri et al., *Dark Energy Survey Year 3 results: Cosmology from cosmic shear and robustness to modeling uncertainty*, Phys. Rev. D **105** (2022) 023515 [2105.13544].

[12] R. Dalal, X. Li, A. Nicola, J. Zuntz, M.A. Strauss, S. Sugiyama et al., *Hyper suprime-cam year 3 results: Cosmology from cosmic shear power spectra*, *Physical Review D* **108** (2023) .

[13] X. Li, T. Zhang, S. Sugiyama, R. Dalal, R. Terasawa, M.M. Rau et al., *Hyper suprime-cam year 3 results: Cosmology from cosmic shear two-point correlation functions*, 2304.00702.

[14] S.-S. Li, H. Hoekstra, K. Kuijken, M. Asgari, M. Bilicki, B. Giblin et al., *KiDS-1000: Cosmology with improved cosmic shear measurements*, A&A **679** (2023) A133 [2306.11124].

[15] Dark Energy Survey and Kilo-Degree Survey Collaboration, T.M.C. Abbott, M. Aguena, A. Alarcon, O. Alves, A. Amon et al., *DES Y3 + KiDS-1000: Consistent cosmology combining cosmic shear surveys*, *The Open Journal of Astrophysics* **6** (2023) 36 [2305.17173].

[16] C.D. Leonard, M.M. Rau and R. Mandelbaum, *Photometric redshifts and intrinsic alignments: Degeneracies and biases in the 3 ×2 pt analysis*, Phys. Rev. D **109** (2024) 083528 [2401.06060].

[17] A. Amon and G. Efstathiou, *A non-linear solution to the S_8 tension?*, MNRAS **516** (2022) 5355 [2206.11794].

[18] G.F. Abellán, R. Murgia and V. Poulin, *Linear cosmological constraints on two-body decaying dark matter scenarios and the S_8 tension*, Phys. Rev. D **104** (2021) 123533 [2102.12498].

[19] Ž. Ivezić, S.M. Kahn, J.A. Tyson, B. Abel, E. Acosta, R. Allsman et al., *LSST: From Science Drivers to Reference Design and Anticipated Data Products*, ApJ **873** (2019) 111 [0805.2366].

[20] O. Doré, C. Hirata, Y. Wang, D. Weinberg, T. Eifler, R.J. Foley et al., *Wfirst: The essential cosmology space observatory for the coming decade*, 1904.01174.

[21] Euclid Collaboration, Y. Mellier, Abdurro'uf, J.A. Acevedo Barroso, A. Achúcarro, J. Adamek et al., *Euclid: I. Overview of the Euclid mission*, A&A **697** (2025) A1 [2405.13491].

[22] A.H. Wright, B. Stölzner, M. Asgari, M. Bilicki, B. Giblin, C. Heymans et al., *Kids-legacy: Cosmological constraints from cosmic shear with the complete kilo-degree survey*, A&A (2025) .

[23] DESI Collaboration, A. Aghamousa, J. Aguilar, S. Ahlen, S. Alam, L.E. Allen et al., *The DESI Experiment Part II: Instrument Design*, *arXiv e-prints* (2016) arXiv:1611.00037 [1611.00037].

[24] DESI Collaboration, B. Abareshi, J. Aguilar, S. Ahlen, S. Alam, D.M. Alexander et al., *Overview of the Instrumentation for the Dark Energy Spectroscopic Instrument*, AJ **164** (2022) 207 [2205.10939].

[25] X. Li, H. Miyatake, W. Luo, S. More, M. Oguri, T. Hamana et al., *The three-year shear catalog of the subaru hyper suprime-cam ssp survey*, *Publications of the Astronomical Society of Japan* **74** (2022) 421–459.

[26] H. Aihara, Y. AlSayyad, M. Ando, R. Armstrong, J. Bosch, E. Egami et al., *Second data release of the Hyper Suprime-Cam Subaru Strategic Program*, PASJ **71** (2019) 114 [1905.12221].

[27] H. Aihara, Y. AlSayyad, M. Ando, R. Armstrong, J. Bosch, E. Egami et al., *Third data release of the hyper suprime-cam subaru strategic program*, *Publications of the Astronomical Society of Japan* **74** (2022) 247–272.

[28] T. Zhang*, S. Sugiyama, S. More, R. Mandelbaum, X. Li, R. Dalal et al., *Modelling Galaxy Clustering and Tomographic Galaxy-Galaxy Lensing with HSC Y3 and SDSS using the Point-Mass Correction Model and Redshift Self-Calibration*, *arXiv e-prints* (2025) arXiv:2507.01377 [2507.01377].

[29] T. Zhang*, X. Li, S. Sugiyama, R. Mandelbaum, S. More, R. Dalal et al., *Cosmology and Source Redshift Constraints from Galaxy Clustering and Tomographic Weak Lensing with HSC Y3 and SDSS using the Point-Mass Correction Model*, *arXiv e-prints* (2025) arXiv:2507.01386 [2507.01386].

[30] M. Tanaka, J. Coupon, B.-C. Hsieh, S. Mineo, A.J. Nishizawa, J. Speagle et al., *Photometric redshifts for hyper suprime-cam subaru strategic program data release 1*, *Publications of the Astronomical Society of Japan* **70** (2017) .

[31] A.J. Nishizawa, B.-C. Hsieh, M. Tanaka and T. Takata, *Photometric redshifts for the hyper suprime-cam subaru strategic program data release 2*, 2003.01511.

[32] M. Tanaka, *Photometric redshift with bayesian priors on physical properties of galaxies*, *The Astrophysical Journal* **801** (2015) 20.

[33] M.M. Rau, R. Dalal, T. Zhang, X. Li, A.J. Nishizawa, S. More et al., *Weak lensing tomographic redshift distribution inference for the hyper suprime-cam subaru strategic program three-year shape catalogue*, Monthly Notices of the Royal Astronomical Society **524** (2023) 5109–5131.

[34] D. Rana, S. More, H. Miyatake, S. Sugiyama, T. Zhang and M. Shirasaki, *Hyper suprime-cam y3 results: photo-z bias calibration with lensing shear ratios and cosmological constraints from cosmic shea*, *Physical Review D* (2025) [2508.21681].

[35] A. Lewis and A. Challinor, "CAMB: Code for Anisotropies in the Microwave Background." Astrophysics Source Code Library, record ascl:1102.026, Feb., 2011.

[36] G. Arico', R. Angulo and M. Zennaro, *Accelerating large-scale-structure data analyses by emulating boltzmann solvers and lagrangian perturbation theory*, Open Research Europe **1** (2022) 152.

[37] J. Hartlap, P. Simon and P. Schneider, *Why your model parameter confidences might be too optimistic. Unbiased estimation of the inverse covariance matrix*, A&A **464** (2007) 399 [astro-ph/0608064].

[38] M. Karamanis, F. Beutler, J.A. Peacock, D. Nabergoj and U. Seljak, *Accelerating astronomical and cosmological inference with preconditioned monte carlo*, *Monthly Notices of the Royal Astronomical Society* **516** (2022) 1644.

[39] M. Karamanis, D. Nabergoj, F. Beutler, J.A. Peacock and U. Seljak, *pocomc: A python package for accelerated bayesian inference in astronomy and cosmology*, *arXiv preprint arXiv:2207.05660* (2022) .

[40] A. Lewis, *Getdist: a python package for analysing monte carlo samples*, Journal of Cosmology and Astroparticle Physics **2025** (2025) 025.

[41] S.R. Hinton, *ChainConsumer*, The Journal of Open Source Software **1** (2016) 00045.

[42] T. Louis, A.L. Posta, Z. Atkins, H.T. Jense, I. Abril-Cabezas, G.E. Addison et al., *The atacama cosmology telescope: Dr6 power spectra, likelihoods and λcdm parameters*, 2503.14452.

[43] A. Amon, D. Gruen, M. Troxel, N. MacCrann, S. Dodelson, A. Choi et al., *Dark energy survey year 3 results: Cosmology from cosmic shear and robustness to data calibration*, Physical Review D **105** (2022) .

[44] L. Secco, S. Samuroff, E. Krause, B. Jain, J. Blazek, M. Raveri et al., *Dark energy survey year 3 results: Cosmology from cosmic shear and robustness to modeling uncertainty*, Physical Review D **105** (2022) .

[45] J. Jefferson, Y. Omori, C. Chang, S. Agarwal, J. Zuntz, M. Asgari et al., *Reanalysis of stage-iii cosmic shear surveys: A comprehensive study of shear diagnostic tests*, The Open Journal of Astrophysics **8** (2025) .

[46] E. Di Valentino, L.A. Anchordoqui, Özgür Akarsu, Y. Ali-Haimoud, L. Amendola, N. Arendse et al., *Cosmology intertwined iii: fσ8 and s8*, Astroparticle Physics **131** (2021) 102604.

[47] Y. Mellier, Abdurro'uf, J.A. Acevedo Barroso, A. Achúcarro, J. Adamek, R. Adam et al., *Euclid: I. overview of the euclid mission*, A&A **697** (2025) A1.

[48] J. Zuntz, M. Paterno, E. Jennings, D. Rudd, A. Manzotti, S. Dodelson et al., *Cosmosis: Modular cosmological parameter estimation*, Astronomy and Computing **12** (2015) 45–59.

[49] J.D. Hunter, *Matplotlib: A 2d graphics environment*, Computing in Science & Engineering **9** (2007) 90.

[50] C.R. Harris, K.J. Millman, S.J. van der Walt, R. Gommers, P. Virtanen, D. Cournapeau et al., *Array programming with NumPy*, Nature **585** (2020) 357.